Applied Catalysis B: Environmental 310 (2022) 121296

Contents lists available at ScienceDirect

Applied Catalysis B: Environmental

journal homepage: www.elsevier.com/locate/apcatb

Evolution behavior and active oxygen quantification of reaction mechanism on cube Cu_2O for CO self-sustained catalytic combustion and chemical-looping combustion

Running Kang [a,b,c], Junqin Huang [a,b], Feng Bin [a,b,*], Zihao Teng [a,d], Xiaolin Wei [a,b], Baojuan Dou [d,**], Saravanan Kasipandi [c,**]

[a] State Key Laboratory of High-Temperature Gas Dynamics, Institute of Mechanics, Chinese Academy of Sciences, Beijing 100190, PR China
[b] School of Engineering Science, University of Chinese Academy of Sciences, Beijing 100049, PR China
[c] Department of Chemical and Metallurgical Engineering, School of Chemical Engineering, Aalto University, Kemistintie 1, P.O. Box 16100, Espoo FI-00076, Finland
[d] Tianjin University of Science & Technology, Tianjin 300457, PR China

ARTICLE INFO

Keywords:
Cube Cu_2O
Active oxygen species
CO
Catalytic combustion
Chemical-looping combustion

ABSTRACT

Catalytic combustion (CC) and chemical looping combustion (CLC) are promising technologies for energy saving and emission reduction of CO_2 in treatment of steelmaking off-gas. This work firstly reports and compares the evolution behavior and quantitative reaction mechanisms of cube Cu_2O model catalyst for CC and CLC reactions. The Cu_2O-CC exhibited the higher activity and stability than Cu_2O-CLC. The typical characterization results suggested that the only surface unstable Cu_2O was oxidized to CuO, and the excellent synergistic effect of metal-oxide interface (100) between Cu^+/Cu^{2+} and active lattice oxygen species for Cu_2O-CC reaction. But, for CLC reaction, Cu_2O structure was collapsed, which caused the agglomeration of CuO_x species and gradual decrease of reaction stability. Three different active oxygen species (surface cycle lattice oxygen, bulk lattice oxygen, and adsorbed oxygen) and the detailed reaction pathways were proposed by the *in situ* IR spectroscopy, isotopic ($^{18}O_2$) transient exchange experiments and DFT simulation. The intrinsic activity of surface cycle lattice oxygen was higher in terms of TOF (13.5×10^{-3} s^{-1}) and facile formation of $C^{16}O^{18}O$ on the cubic interface of Cu_2O-CC through adsorbed CO during CC process. The contribution degrees of Mars-van-Krevelen (M-K) and Langmuir–Hinshelwood (L-H) mechanisms for CC and CLC reactions were 76.6% and 23.4% for CC, and 89.7% and 10.3% for CLC on Cu_2O catalyst, respectively.

1. Introduction

A considerable amount of emitted off-gas (CO≤35%, O_2 ≥2%) at steelmaking plants cannot be considered directly as standard fuel, because its CO+O_2 mixtures tend to cause explosions, that usually discharged into environment by methane combustion supporting way through exhaust tower. In general, the off-gas accounts for about 20% of the total gas and consumes millions of CH_4 each year, resulting in the more energy waste as well as extra emission of CO_2. To reduce the emission of CO_2 before 2030 and carbon neutral by 2060 in China, therefore, developing an essential effective combustion technologies such as catalytic combustion (CC) and chemical looping combustion (CLC) is actively studying by many research groups [1–3]. As for CC (Fig. 1A), the CO self-sustained catalytic combustion can be determined by our group *via* CO→CO_2 exothermic reaction, where the CO is effectively oxidized in presence of air to CO_2 over the catalytic reactor at low ignition-temperature [4]. When the catalytic converter warms up to its ignition temperature, the sudden self-acceleration of the surface rate leads to a thermochemical runaway, followed by a rapid transition to self-sustained catalytic combustion. The identified scenario can be applied in the recovery of chemical heat in steelmaking off-gas systems. But both fuel and air reactors are used in the CLC to avoid the direct contact between CO and air (Fig. 1B). In more details, the CO is converted into CO_2 *via* fuel reactor by lattice oxygen donated from catalysts

* Corresponding author at: State Key Laboratory of High-Temperature Gas Dynamics, Institute of Mechanics, Chinese Academy of Sciences, Beijing 100190, PR China.
** Corresponding authors.
E-mail addresses: binfeng@imech.ac.cn (F. Bin), bjdou@tust.edu.cn (B. Dou), Saravanan.Kasipandi@vtt.fi, ksarvanchem@gmail.com (S. Kasipandi).

https://doi.org/10.1016/j.apcatb.2022.121296
Received 14 December 2021; Received in revised form 15 February 2022; Accepted 5 March 2022
Available online 8 March 2022

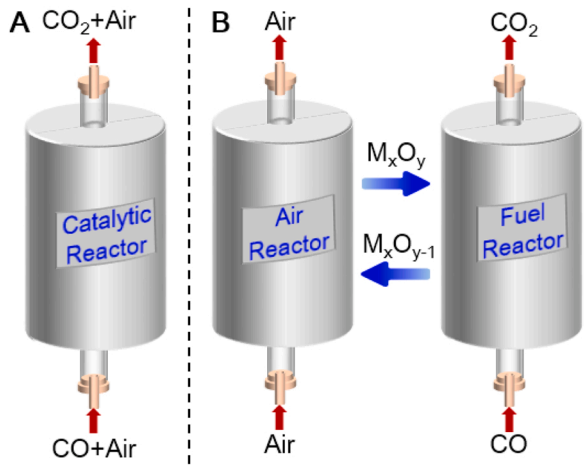

Fig. 1. Diagram of the CO catalytic combustion (A) and chemical looping combustion (B) processes.

or oxygen carrier (M_xO_y), beneficial for inherent CO_2 separation and capture [5]. Subsequently in air reactor, the reduced catalysts/oxygen carrier (M_xO_{y-1}) could recuperate its oxygen capacity by absorbing O_2 from air. As such, the CC reaction process can be seemed as many CLC processes composition although the former is not easy to separate CO_2.

There have been many publications in Cu-based catalysts for both CC or CLC processes because of their potential activity inspired by the suitable active sites and oxygen storage-release capacity [6–8]. The reaction behaviors on such catalyst including structure-activity relationship and stable active center are crucial for the CC and CLC processes. Special attention is currently drawn to the structure evolution and active oxygen function of the model catalysts, which in turn restrict the activity in comparative CC and CLC reactions. With respect to CC reaction process, based on the Cu, Cu_2O and CuO catalysts, Huang et al. [9] provided evidence that the non-stoichiometric metastable copper oxide species formed over the Cu_2O exhibit an excellent transportation of surface lattice oxygen and catalytic activity. The catalytic ignition of CO includes kinetics and heat generation since the heat produced is governed by the reaction kinetics. Correspondingly, a transition from low-reactivity steady state to high-reactivity steady state can be observed due to heat transfer limitation, which exhibits different reaction stages. In our group, the evolution of active sites was obtained from intrinsic reaction kinetics stage on the Cu^+-$[O_v]$-Ce^{3+} to self-sustaining catalytic combustion stage over the surface Cu^+ site at high CO concentrations [10,11]. By means of Cu_2O with regular morphology, we also confirmed that the unsaturated coordination of Cu and O on the different planes can enhance the corresponding reducibility, adsorption and activation of gaseous oxygen, consequently promoting the CO oxidation to CO_2 [12]. Similar result was also obtained by Hua et al. They observed that the unsaturated Cu^I of Cu_2O nanocrystals are most active sites in chemisorbing and catalyzing CO oxidation through CC reaction [13]. By comparison, the CLC exhibits only the kinetic behavior of catalyst, which corresponds to a low reaction rate. Goldstein and Mitchell measured the kinetic parameters of copper oxides (pure CuO and Cu_2O) reduction by CO in a pressurized TGA, and revealed overall activation energy for the reduction of CuO and Cu_2O to Cu, respectively [14]. Christopher et al. suggested that the oxidation kinetics of Cu_2O depend on grain boundaries sintering and the oxygen generation ability at oxygen partial pressure under different temperature [15]. However, the results on actual structure evolution behaviors (intrinsic structure-performance relationship and effective interface position) of Cu_2O model catalysts during the CC and CLC processes are rarely reported so far.

A complete fundamental understanding about the types and nature of active oxygen species is important for correctly establishing the detailed CO reaction mechanism, which is the focus of the current study. Up to now, the active oxygen species in macroscopic mechanism of Cu_2O for the CC and CLC were only studied by the qualitative analysis. For instance, Su. et al. shown that O_2 easily chemisorbed on the Cu_2O surface to form Cu—O bond and Cu^{2+} cations were gradual outward surface diffusion with Cu_2O oxidation mechanism in the CLC process, whereas the function of various oxygen species was not reported [16]. The beneficial effort of reaction pathway in the CC reaction was carried out by Zhang et al. [17]. They proved that CO oxidation follows both M-K and L-H mechanisms on the Cu_2O (100) *via* density functional theory (DFT) calculation, in which lattice oxygen and adsorbed oxygen species reacted with the adsorbed CO. According to our previous work, M-K mechanism was proposed for the CO self-sustained catalytic combustion over the Cu_2O catalyst through CO-TPD-MS analysis, where adsorbed CO mainly reacts with lattice oxygen [12]. But the calculated E-R mechanism involving gaseous oxygen in CO oxidation was found to be more feasible than the M-K (lattice oxygen) and L-H mechanisms (adsorbed oxygen) on the Cu_2O and the CuO surface model due to the different adsorbed energy of oxygen species in the CC reaction[18], which is quite different from previous knowledge. In order to bridge the gap between qualitative analysis and quantitative analysis, Chen et al. made a semi-quantitative result based on the relative intensity change of DRIFT peaks to reveal the reaction pathway, where the adsorbed CO mainly reacts with surface lattice oxygen from Cu^+-$[O_v]$-Ce^{3+} interface [19]. However, it is still difficult to clarify reaction rates of different active oxygen species on the copper active sites due to the sensitivity of infrared absorption/transmission peaks in the transition state species was different. So far, there is a little direct evidence using the actual *in situ* experiments to reveal the function of different oxygen species with reaction pathways in quantitative way, resulting in no common perception for the contribution of reaction mechanisms in the CC and CLC. Moreover, the published results for the active sites and calculated mechanisms over the Cu_2O catalyst for either CC or CLC processes. Nevertheless, the evolution behaviors of Cu_2O structural changes, valence states of Cu species and active oxygen species in both CC and CLC processes are still scarce. In this sense, it is necessary to clarify the aforementioned two issues by using Cu_2O model catalysts during both CC and CLC processes. Fortunately, our work provides enough evidence on the evolution behaviors and quantitative reaction pathways of cubic Cu_2O during the CC and CLC process to determine those crucial parameters.

The present investigation firstly identifies the various evolution behaviors clearly including Cu_2O structure change, structure-activity relationship, and active interface between copper species and active oxygen species by using fresh and used cubic Cu_2O model catalysts in both CC and CLC processes. Particularly, the active oxygen species from active sites and the contribution degree of different active oxygen species to reaction mechanisms are distinguished *via in situ* infrared (IR) and unique isotopic ($^{18}O_2$) transient exchange experiments as well as DFT calculation. Secondly, the amount of active oxygen species and dynamic turnover frequency (TOF) are calculated to evaluate those reaction processes. As a promising research topic, this work aims to bridge the missing gap, and the evolution behaviors and fundamental quantitative reaction mechanism between the comparative CC and CLC reactions over cubic Cu_2O catalyst. The obtained fundamental results are beneficial to make a comprehensive understanding of the actual surface reaction process on cubic Cu_2O catalyst, and provide theoretical support to the advanced catalyst design and intrinsic mechanism research for CC and CLC reaction processes.

2. Experimental specifications

2.1. Synthesis of the catalyst

All chemical reagents were used as analytical grade and without further purification. In liquid-phase reduction method, as shown in

Fig. S1A, $CuCl_2.2\ H_2O$ (1.7 g) was dissolved in ultrapure water (1.0 L), which was stirred at 55 °C for 0.5 h to get transparent light green $CuCl_2$ solution (0.01 mol/L). Then aqueous solution of NaOH (100 mL, 2.0 mol/L) was added dropwise to the above solution to obtain a dark brown suspended solution, flowed by ascorbic acid (100 mL, 0.6 mol/L) was added slowly. The obtained solution was stirred at 55 °C for 5 h and gradually formed turbid red solid precipitate. The resulting precipitate was collected by washing with ultrapure water three times until the solution reached neutral condition. Prior to obtain fresh cubic Cu_2O catalyst, the catalytic sample was washed with absolute ethanol to remove the residual inorganic ions and polymer, and was dried in vacuum oven at 60 °C for 12 h.

2.2. Characterization of fresh and used catalysts, and in situ studies

X-ray powder diffraction (XRD) of the fresh Cu_2O and, used Cu_2O-CC and Cu_2O-CLC were recorded on an XD-3-automatic diffractometer (PERSEE) using Cu Kα radiation as the radiation source. X-ray photoelectron spectroscopy (XPS) measurements on the fresh Cu_2O and, used Cu_2O-CC and Cu_2O-CLC catalysts were performed with a Kratos Axis Ultra DLD spectrometer. Scanning electron microscopy (SEM) image was acquired with a Hitachi S-4800 to observe the overall morphology of the fresh Cu_2O and, used Cu_2O-CC and Cu_2O-CLC samples. Temperature programmed reduction (H_2-TPR and O_2-TPD) was conducted for both fresh and used Cu_2O samples by a chemisorption analyzer (TP5080B). For the H_2-TPR studies, each sample (20 mg) was reduced under the H_2 atmosphere (30 mL/min), with the temperature increasing from room temperature to 600 °C at 10 °C/min. On the other hand, for O_2-TPD, each sample (20 mg) was heated and maintained with 300 °C for 30 min in a He atmosphere (30 mL/min). After that each sample was adsorbed with O_2 for 1 h at room temperature and then flush with He for 0.5 h (30 mL/min). Then reactor was heated to 950 °C at a rate of 10 °C/min. *In situ* IR experiment was performed on the FOLI10-R instrument (INSA Optics Instruments (Shanghai) Ltd.) coupled with a self-designed magnetically driven transmission cell, where approximately 5 mg of catalyst and 50 mg KBr were mixed and pressed into a self-supporting wafer. Prior to recording IR spectra, the sample was pretreated in a N_2 flow at 300 °C. Isotopic ($^{18}O_2$) exchange experiments were conducted with the *in situ* fixed-bed reactor, which was attached with online mass spectrometer (MS, Pfeiffer Omnistar™) to identify the detailed oxygen species exchange process. To ensure steady transient operation, eliminate the effect of dead volume and obtain transient response signal of reactants and products, four-way switch valve was firstly applied to switch the gas paths quickly and maintain continuous flow of reactant gases as shown in Fig. S1B. The sample (30 mg) was pretreated in an *in situ* fixed-bed reactor at 300 °C for 20 min with Ar atmosphere (30 mL/min). Then the flowing reactant gases (30 mL/min, 10 vol% CO+21 vol% $^{18}O_2$/Ar for CC, 10 vol% CO/Ar and 21 vol% $^{18}O_2$/Ar for CLC) were constantly pulsed into the reactor at 300 °C and the isotopic products were monitored by the online MS. The concentration of gases was calibrated by gas analyzer and converted them based on MS intensity signals. The isotopic gas of 21 vol% $^{18}O_2$/Ar was provided by WUHAN NEWRADAR SPECIAL GAS Co., LTD.

2.3. Catalytic activity test

The catalytic activity of Cu_2O was evaluated in a fixed-bed flow reactor for CC (10 vol% CO+21 vol% O_2/Ar) and CLC (10 vol% CO/Ar, and 21 vol% O_2/Ar) processes. A powdered catalyst (~200 mg) was loaded into a quartz tube reactor (i.d. 4 mm), and the flow rates of CO, O_2 and N_2 (0.2 L/min) were controlled by mass flow controllers (± 1% FS). The catalyst was pretreated in Ar at 200 °C for 2 h and cooled to room temperature. Then the catalyst was heated from room temperature to the desired reaction temperature of 350 °C at 10 °C/min. The temperature distributions of the reactor surface were detected by a forward-looking infrared radiometer (FLIR, T640, USA) after realizing CO self-sustained combustion, with a certain glass emission rate (0.87). The effluent gas was analyzed with an online multicomponent analyzer (QGS-08 C for CO/CO_2 and OGS-10 T for O_2, Maihak). The 3–5 cycle tests of Cu_2O were also presented at a steady reaction state with different temperature points for CC and CLC, and the exhaust gas was detected using an online MS.

2.4. DFT simulations

The calculation method was performed by using Dmol^3 package with spin-polarized DFT [20]. All calculations were conducted using the generalized gradient approximation (GGA) of the Perdew–Burke–Ernzerhof (PBE) exchange-correlation functional [21,22]. 0.005 Ha Fermi smearing parameter was adopted in the calculations. Convergent values were set as 2.0×10^{-3} Ha/Å (force), 10^{-5} Ha (energy), and 5.0×10^{-3} Å (displacement). The Brillouin zones of the Cu_2O (100) surfaces were sampled with $3 \times 3 \times 1$ Monkhorst Pack **k**-point meshes. The optimized bulk lattice constants of Cu_2O are a=b=c= 4.2696 Å and the 2×2 supercell model is performed in Fig. S2, which is consistent in the result of Hssi et al. (4.26 Å) [23].

The adsorption energy (E_{ads}) can be calculated by Eq. (1):

$$E_{ads}=E_{adsorb\text{-}sub}- E_{adsorb}- E_{sub} \quad (1)$$

where E_{adsorb}, E_{sub} and $E_{adsorb\text{-}sub}$ represent the energies of adsorbate, the catalyst model, and the adsorption system after optimization, respectively. A large negative value of E_{ads} represents strong adsorption strength.

The reaction pathway of CO oxidation over the Cu_2O surface is connected by initial state (IS), intermediate (IM), transition state (TS) and final state (FS). The complete linear synchronous transit and quadratic synchronous transit (LST/QST) method was applied for the transition states searching [24]. Only one imaginary frequency exists for all transition states, which is confirmed through vibrational frequency analysis. The reaction energy barrier (E_a) can be calculated as:

$$E_a = E_{TS} - E_{IM} \quad (2)$$

where E_{TS} represents the energy of transition state, and E_{IM} is the energy of intermediate.

3. Results and discussion

3.1. Catalytic combustion and chemical-looping combustion reaction

The activity of cubic Cu_2O was evaluated for both catalytic combustion and chemical-looping combustion, as shown in Fig. 2A. The light-off profile for CC and CLC reactions were obtained and recorded each point during the temperature-programmed process (from room temperature to 350 °C at 10 °C/min) by using fresh Cu_2O catalyst. The CO is easy to be ignited by addition of gaseous O_2 during catalytic combustion (labeled as Cu_2O-CC). The values of T_{10} and T_{100} (corresponding to 10% and 100% CO conversion, respectively) on Cu_2O are 182 and 201 °C, respectively, which are lower than that of Cu_2O in chemical-looping combustion (marked as Cu_2O-CLC) (T_{10} = 255 °C, T_{100} =335 °C). Particularly, the steady CO self-sustained combustion is achieved over Cu_2O-CC due to the heat transfer limitation, with the hot zone temperature of 182.8 °C in reactor bed, which was already verified in our previous study [4,6,12]. When the catalytic converter warms up to its ignition temperature (T_{10}), the sudden self-acceleration of the surface rate leads to a thermochemical runaway, followed by a rapid transition to realize self-sustained catalytic combustion. By comparison, the activation of lattice oxygen in Cu_2O-CLC without addition of external gaseous O_2 needs a higher reaction temperature to convert CO completely, so that the self-sustained combustion cannot be realized here because the active lattice oxygen from CuO_x species consumes gradually. The calculated activation energies (Fig. 2B) reveals that the

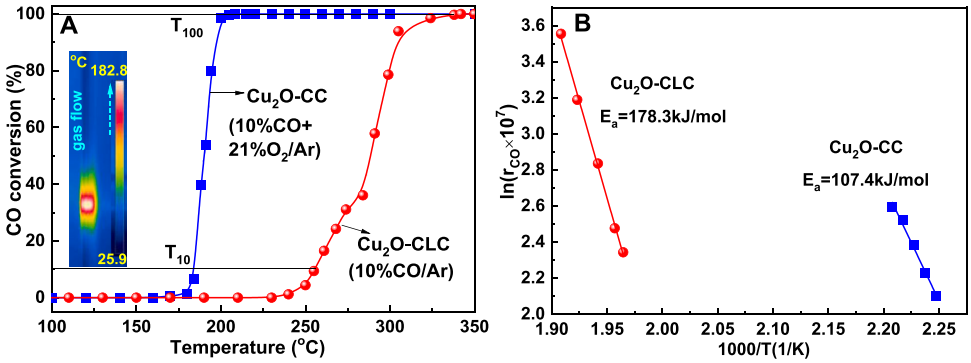

Fig. 2. The catalytic activity and activation energy profiles for Cu_2O-CC and Cu_2O-CLC processes.

energy barrier of Cu_2O-CC (107.4 kJ/mol) is lower than that of Cu_2O-CLC (178.3 kJ/mol), which is similar in the literature [12]. For comparison, the catalytic activity results on cubic Cu_2O and reported Cu_2O and CuO/CeO_2 catalysts were listed in Table S1. This work aims to bridge the missing gap between CC and CLC reactions in understanding the evolution behaviors and quantitative reaction mechanism over cubic Cu_2O catalyst, although reported CuO/CeO_2 catalyst show a good activity for CO oxidation.

Fig. 3 presents the step-response runs of fresh Cu_2O for CC and CLC processes. The CO completely converted into CO_2 at $\geq$ 300 °C with stable high CO→CO_2 reaction rate after 5 min (Fig. 3A, 10 vol% CO + 21 vol% O_2/Ar), although no conversion of CO was occurred at 100 °C as predicted. Such a stable combustion has also confirmed by 3-cycle tests at 300 °C (Fig. S3), with no apparent difference in position and tendency of CO, CO_2 and O_2 curves observed. Fig. 3B illustrates the 5-cycle performance of Cu_2O in chemical looping combustion. Each cycle consists of a CO oxidation reaction with oxygen in Cu_2O by 10 vol % CO/Ar, followed by oxidation of sample to supply oxygen *via* 21 vol% O_2/Ar. The activity of Cu_2O-CLC was decreased in each cycle at 300 and 500 °C especially after the first two cycles, which was clearly indicated in an increasing initial concentration of CO, and thus no formation of CO_2. Similarly, the O_2 concentration also decreased over the successive reaction cycles. This phenomenon may be due to oxidation of Cu^+ to Cu^{2+} during Cu_2O-CLC process. It can be seen that the formation of CO_2 was superior at 300 °C, which is selected for isotopic ($^{18}O_2$) exchange experiments as well as mechanism investigation studies. To clearly understand the structural and physicochemical property changes on Cu_2O in both Cu_2O-CC and Cu_2O-CLC processes, we thoroughly assessed fresh and used Cu_2O catalysts and discussed in the next section.

3.2. *Structural and chemical state characterizations on fresh and used Cu_2O*

The XRD analysis was performed to identify crystallinity and structural changes of the catalysts. As shown in Fig. 4, the fresh Cu_2O displayed a typical diffraction peaks at 29.6°, 36.4 °, 42.3 °, 61.5 °, and 73.7 °for cubic phase of Cu_2O (JCPDS No. 99-0041) [25]. After catalytic combustion test on Cu_2O (Cu_2O-CC), the diffraction peaks for cubic Cu_2O were almost retained, although the intensity of all peaks were decreased besides appearance of two additional weak peaks at 35.5° and 38.7° for CuO species (JCPDS card No. 45-0937), which were indicated that a small surface Cu_2O fractions are unstable and can tend to be

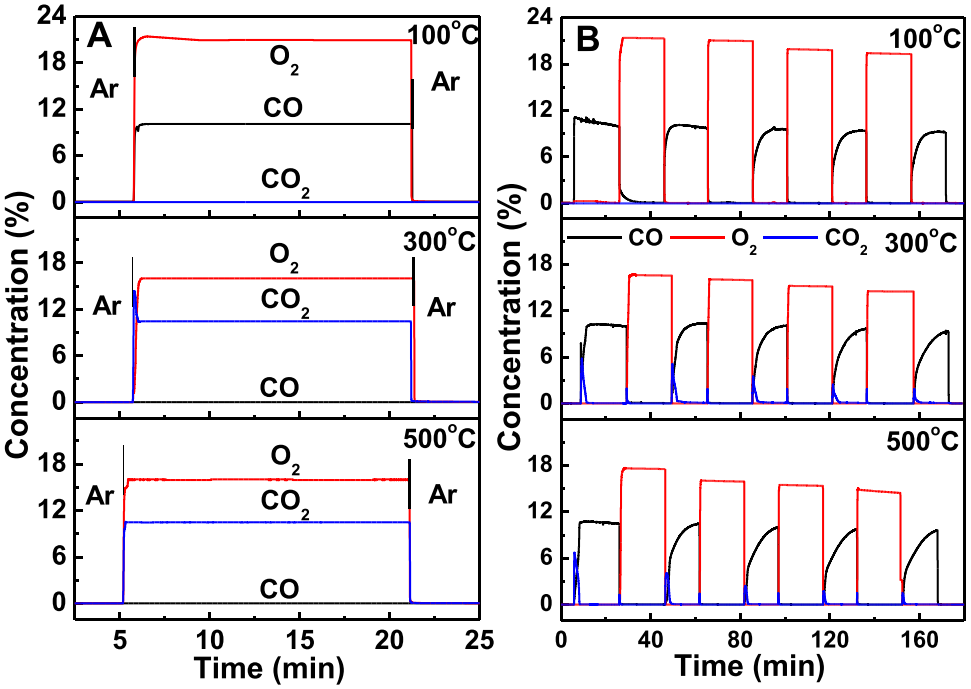

Fig. 3. (A) Catalytic combustion over Cu_2O-CC (with 10 vol% CO + 21 vol% O_2/Ar) and (B) chemical looping combustion (with 10 vol% CO/Ar and 21 vol%O_2/Ar) over Cu_2O-CLC catalyst at different temperatures and time.

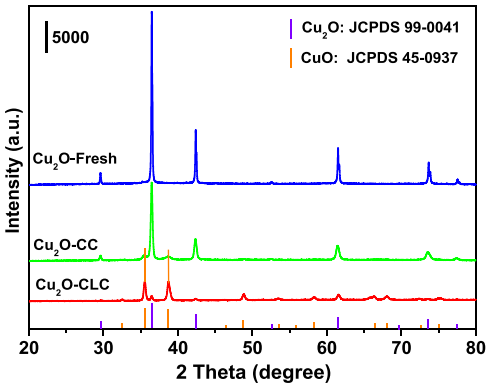

Fig. 4. XRD patterns of the fresh Cu_2O, used Cu_2O-CC and Cu_2O-CLC catalysts.

oxidized to a CuO during CC process. After CLC, however, the diffraction peaks of cubic Cu_2O were nearly disappeared and strong diffraction peaks for CuO species attributed to agglomerate CuO species were formed. Apparently, the cubic Cu_2O structure was destroyed since most surface and bulk Cu_2O was oxidized into CuO species during CLC.

Fig. 5 illustrates the SEM images and 3D reconstruction of the surface morphology of fresh Cu_2O, used Cu_2O-CC and Cu_2O-CLC catalysts. Particularly, the images with big scale of all catalysts were also obtained as shown in Fig. S4. Interestingly the cubic Cu_2O structure was preserved with smooth surfaces on freshly prepared Cu_2O (Fig. 5A, D and G), which selectively exposes six (100) crystal plane [12,26]. Similarly, as shown in Fig. 5B, the cubic structure with six crystal planes for Cu_2O was retained on Cu_2O-CC. However, a slight rough surface was observed than that of the fresh Cu_2O sample (Fig. 5B, E and H), which clearly showed that a part of small dense grain of surface Cu_2O was oxidized to CuO particulars to supply enough active sites (by cycle of $Cu^{+} \leftrightarrow Cu^{2+}$) during CC process. This is corroborated by the stable adsorption and release of active oxygen to participate in CO oxidation reaction during the reaction equilibrium with excess O_2 (see Fig. 3A). Hence the Cu_2O exhibited the high activity and stable performance in CC, in accordance with the results provided in Figs. 2 and 3A. However, the cubic structure of Cu_2O collapsed after reduction by 10 vol% CO/Ar and cannot realize the significant surface reconstruction although oxidation with 21 vol% O_2/Ar in CLC process (Fig. 5C). The bumpy surface on Cu_2O during CLC was clearly observed as shown in the Fig. 5F and I. This surface change may cause from the consumption of most of active oxygen species on Cu_2O in the reduction process that can form the large internal cavities and optically-visible macroporosity. Similar behavior was also observed for CLC with ilmenite and CuO/(TiO_2, SiO_2, and ZrO_2) [27]. The structural changes on Cu_2O during CLC process (Cu_2O-CLC) after oxidization process were confirmed by both XRD and SEM results, thus the collapse of the cubic structure and agglomeration of CuO cannot provide enough active sites and active oxygen species in Cu_2O-CLC. Such a change leads to continuous consumption of lattice oxygen and the decrease of catalytic activity. Moreover, the observed activity differences over the time for Cu_2O-CC to Cu_2O-CLC (Fig. 3) can more readily

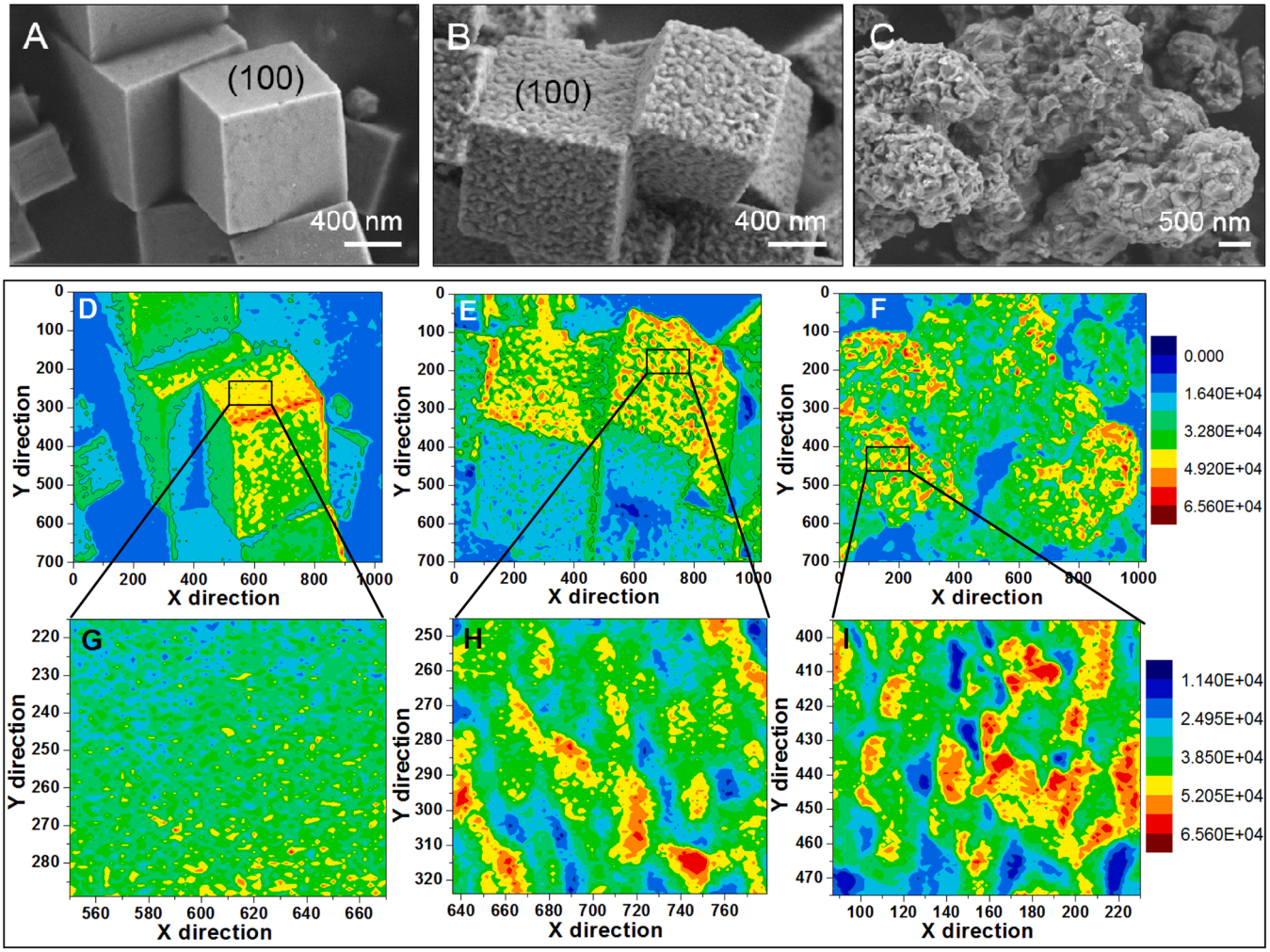

Fig. 5. SEM images and 3D reconstructions of the fresh Cu_2O (A, D and G) and used catalysts for CC (B, E and H) and CLC (C, F and I) processes.

be explained by structure change with decreasing the total perimeter length of the contact boundary between active lattice oxygen species and Cu ions phases. The results provide compelling evidence for structure-activity relationship that this cubic metal-oxide interface provides the most active sites. The migration and reaction process of active lattice oxygen species is further discussed in the isotopic exchange experiments.

To further illustrate the chemical state and composition of elements on the surface of the catalysts, XPS analysis was performed on both fresh and used catalysts as shown in Fig. 6. Then the XPS peaks centered at 932.9 and 935.0 eV (Fig. 6A) are assigned to Cu^{+} ions and Cu^{2+} ions, respectively [28]. The elemental analysis for Cu and O species were calculated and complied in Table 1. As confirmed with XRD pattern, the fresh Cu_2O only contains Cu^{+} species with 35.3 at%, which was decreased by forming Cu^{2+} species after the reaction in both CC and CLC processes. The Cu^{2+} content in Cu_2O-CLC (33.1 at%) was higher than Cu_2O-CC (24.8 at%) which clearly inferred that the former catalytic process on Cu_2O was overoxidized by 21% O_2/Ar ($Cu^0/Cu^{+}\rightarrow Cu^{2+}$) that of later catalytic process. It is interesting that the Cu^{2+} content of Cu_2O-CC was moderate since the cycle of Cu species ($Cu^{+}\leftrightarrow Cu^{2+}$) can be well realized on the Cu_2O-CC surface during CO catalytic combustion, verified by the formation of CuO layer on the Cu_2O-CC surface (Fig. 5B). The Fig. 6B depicts the O 1 s spectra to study the different oxygen species on the surface of fresh and used Cu_2O catalysts. The spectra consists of three peaks located at 529.1 eV, 530.8 eV, and 533.2 eV, which can be assigned to active lattice oxygen in CuO (O_{L2} bonds to metal) and Cu_2O species (O_{L1}), and the surface oxygen defect sites (*e.g.* hydroxyl (O_{OH}) and/or adsorbed oxygen species) [7,29], respectively. It is obvious from Table 1 that the formation of O_{L2} species on used Cu_2O (21.5 at% for Cu_2O-CC and 32.3 at% Cu_2O-CLC) was attributed to the formation of Cu^{2+} ions and transformation of gas phase oxygen into lattice oxygen species during both CC and CLC processes. Particularly, the Cu_2O-CLC was exhibited the higher species of O_{L2} (32.3 at%) and lower species of O_{L1} (16.7 at%), due to its relatively facile transformation of Cu^{+} to Cu^{2+} species with independent excess oxygen oxidizing in chemical looping combustion process.

H_2-TPR experiment was further performed to investigate the change of Cu species on the fresh and used Cu_2O catalysts. As shown in Fig. 7A, the α peak in the Cu_2O-fresh and used Cu_2O-CC was assigned to the reduction of highly dispersed copper ions, whereas the β peak in all catalysts can be assigned to the reduction of bulk copper ions [6]. The new γ and δ peaks on the Cu_2O-CLC at the higher temperature was due to the formation of agglomerated CuO_x species after the deep oxidation during CLC process. Through curve integration, the H_2 consumption at α peak of Cu_2O-fresh was lower than that of Cu_2O-CC (Table 1), since

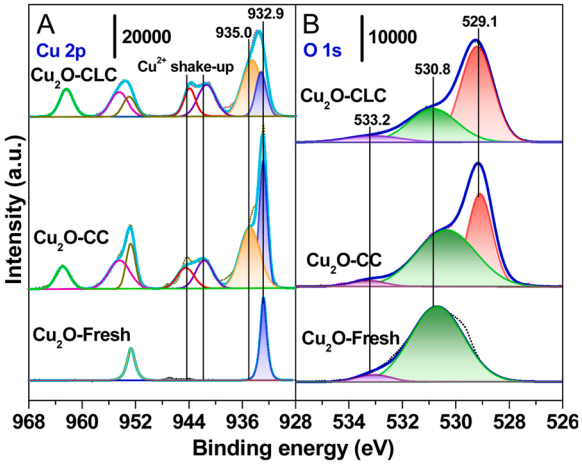

Fig. 6. XPS spectra for Cu 2p (A) and O 1 s (B) on the fresh and used Cu_2O catalysts.

there are less dispersed copper ions on the Cu_2O-fresh catalyst. Whereas the agglomeration of CuO_x species and nearly no dispersed copper ions can be observed on the Cu_2O-CLC, thus the appearance of new γ and δ peaks with much amount of H_2 consumption instead of α peak. Upon comparing the reduction behavior of Cu_2O-CC and Cu_2O-CLC samples, it is evident that Cu_2O-CC was much easier reducible than that of Cu_2O-CLC. We speculated that H_2 spillover from surface to bulk was easily facilitated in Cu_2O-CLC than in Cu_2O-CC.

O_2-TPD was used to study the presence of oxygen species on the catalysts (Fig. 7B). Generally, the oxygen desorption peaks that appeared at low temperature (<300 °C) and high temperature (>300 °C) are attributed to the surface adsorbed oxygen and lattice oxygen species, respectively [30]. Hence the two desorption peaks labeled as α_1 (<100 °C) and α_2 peak (100–300 °C) were also assigned to the physically and chemically adsorbed oxygen species, respectively. Other two high temperature desorption peaks (>300 °C) were assigned to surface (β peak) and bulk (γ peak) lattice oxygen species that binds to metal cations, respectively [29,31]. Owing to the formation of CuO_x species, the chemically adsorbed oxygen peaks on the Cu_2O-CC and Cu_2O-CLC were stronger than that of Cu_2O-fresh, which clearly indicates that gaseous oxygen easily adsorbed on the Cu_2O during both CC and CLC processes. It is important to mention that the peak area of lattice oxygen species was much higher than the adsorbed oxygen species, suggested that lattice oxygen species was played an important role in the CC and CLC processes. The lattice oxygen species is beneficial to promoting the adsorption and activation of gaseous oxygen on the catalyst surface, thus accelerating the CC and/or CLC reaction. The contribution of different active oxygen species to CC or CLC will be further discussed in the following *in situ* IR and isotopic ($^{18}O_2$) exchange experiments.

3.3. *In situ IR and isotopic ($^{18}O_2$) exchange experiments*

To further investigate the intermediates and the reaction behavior in the CC and CLC processes, the *in situ* IR was performed with fresh Cu_2O catalyst (Fig. 8). The intense bands at 2172 and 2118 cm^{-1} are attributed to gaseous CO [6]. In general, CO is adsorbed on the Cu^{+} to form carbonyl bond through coordinatively unsaturated metal sites and oxygen vacancies and then continues with C—O bond activation [32]. Due to the very week interaction of adsorbed CO and O_2, as shown in Fig. 8A, the intensity peak for carbonate species were nearly unobserved at 1350–1750 cm^{-1}. However, when the temperature increases from 30 to 500 °C, the intensity for CO band reduced rapidly without any change in the carbonate species. At the same time, the intensity of CO_2 bands at 2342 and 2361 cm^{-1} increased, indicating that the adsorbed CO on the catalyst surface can easily react with active lattice oxygen of Cu_2O, instead of the decomposition of carbonate species (Fig. 8A and B). Compare with the CO_2 yield in CLC process (Fig. 8C and D), the CC reaction showed the higher activity with more CO_2 yield under 10 vol% CO+ 21 vol% O_2/Ar, assigned to the former not supplying enough active oxygen species in the 10 vol% CO/Ar atmosphere. Such a phenomenon involves an electron donation from carbon (lone pair on 5σ orbital) to d orbitals of the metal cations (Cu^{+}) or an electron back-donation from d orbitals of the metal cations to 2π* -antibonding of carbon [33,34]. The adjacency of the CuO_x adsorption sites to the reactive surface lattice oxygen on the cubic interface available for the subsequent abstraction eventually becomes a key aspect in the activity analysis over Cu_2O-CC in the CC process.

The isotopically labeled $^{18}O_2$ gas is used to mark the three different formed species namely $C^{16}O_2$, $C^{16}O^{18}O$ and $C^{18}O_2$ produced by different active oxygen species. Fig. 9 displayed the reactants and products over Cu_2O in CC (A) and CLC (B) processes at 300 °C. Before the reaction, the fresh Cu_2O was purged and kept in Ar (30 mL/min) at 300 °C. The CO signal was disappeared with decreased of $^{18}O_2$ (about 16 vol%) after switching 10 vol% CO + 21 vol%$^{18}O_2$/Ar as shown in Fig. 9 (A), indicates that the CO was completely oxidized at 300 °C over Cu_2O-CC catalyst, in agreement with activity results. Three CO_2 isotopomers

Table 1
Surface percentage of Cu and O species obtained by XPS, and α, β and γ + δ fractions from H_2-TPR for fresh and used Cu_2O catalysts.

Catalyst	Surface atom percentage (at%)						H_2 consumption (mmol/g)		
	Cu/O	Cu^+	Cu^{2+}	O_{L1}	O_{L2}	O_{OH}	α peak	β peak	γ + δ peak
Cu_2O-fresh	54.6	35.3	–	61.1	–	3.6	0.93	2.75	–
Cu_2O-CC	85.9	21.4	24.8	30.6	21.5	1.7	1.10	2.30	–
Cu_2O-CLC	90.5	14.4	33.1	16.7	32.3	3.5	–	3.15	3.01

O_{L1} and O_{L2} are lattice oxygen of Cu^+ and Cu^{2+} respectively.

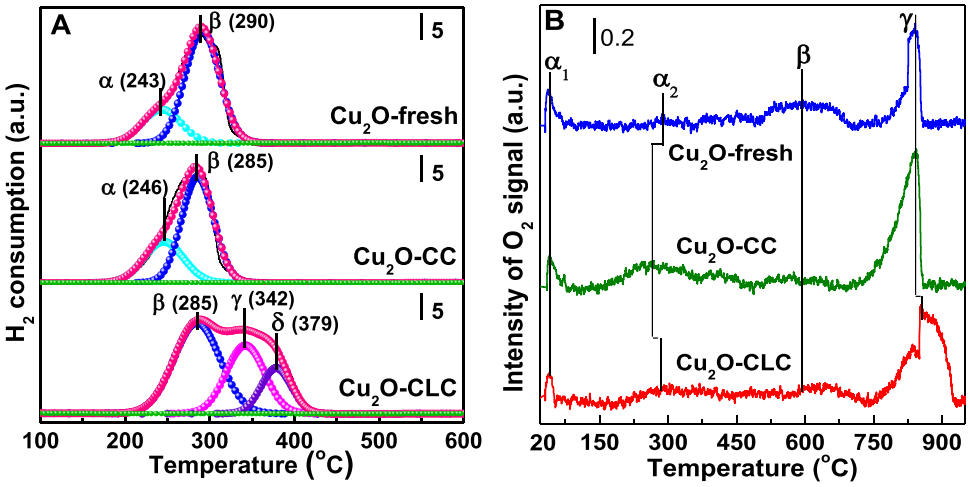

Fig. 7. (A) H_2-TPR and (B) O_2-TPD profiles of the fresh and used Cu_2O catalysts.

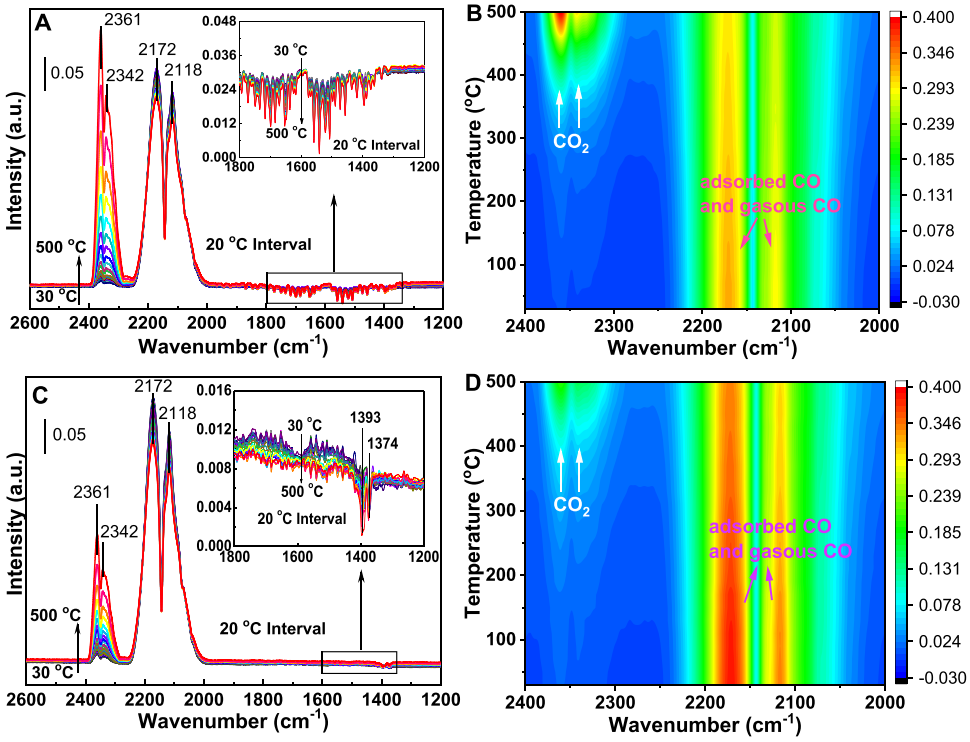

Fig. 8. *In situ* IR spectra of fresh Cu_2O and corresponding mapping results under (A, B) 10 vol% CO+ 21 vol% O_2/Ar, and (C, D) 10 vol% CO/Ar continuous stream.

products with different concentrations were observed in the CC process. Large amounts of $C^{16}O_2$ produced quickly until 7 min, which decreased to 0.7 vol% gradually with increasing time. Then $C^{16}O^{18}O$ produced comparatively and quickly increases to about 6.8 vol%. The $C^{18}O_2$ produced slowly and increased to about 2.3 vol% gradually. It is well known that the Cu_2O precursor was prepared in air atmosphere including $^{16}O_2$, pretreated in Ar atmosphere and reacted in $^{18}O_2$, thus $C^{16}O_2$ is certainly produced *via* lattice oxygen species from Cu^+ ions of the Cu_2O-CC catalyst itself, which is verified by XPS results. The above results obviously evidence that the CO was oxidized by surface lattice

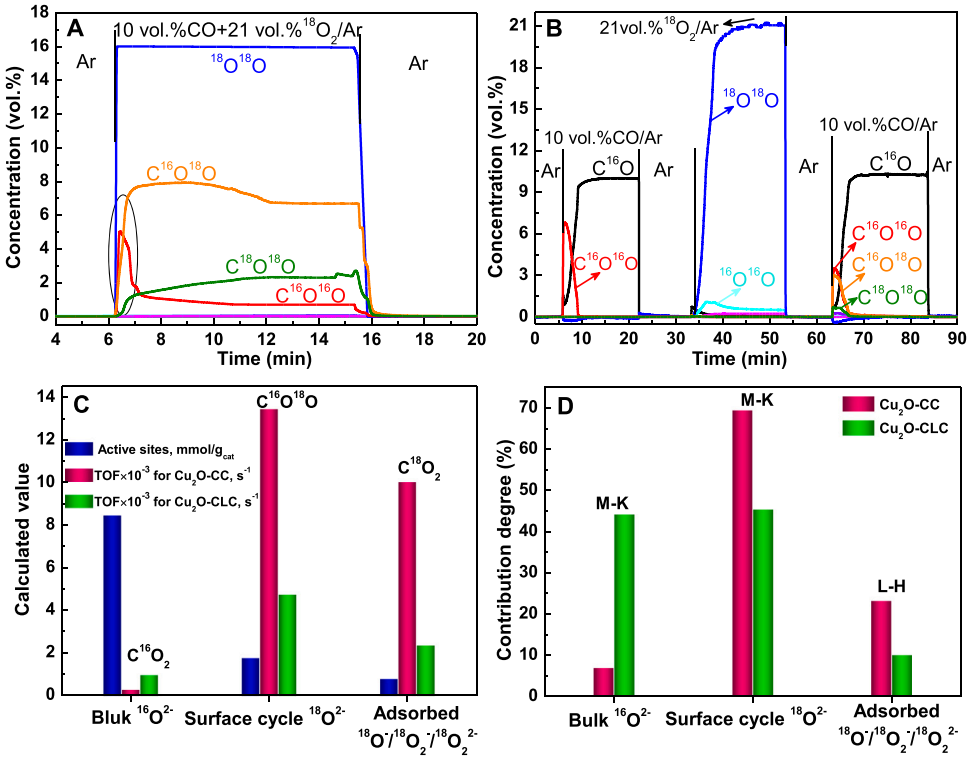

Fig. 9. Isotopic ($^{18}O_2$) exchange experiments over Cu_2O for CC (A) and CLC (B) processes at 300 °C; the amount of different active sites and TOF (C), and contribution degree of different mechanisms on active oxygen species (D) for Cu_2O-CC and Cu_2O-CLC processes.

oxygen ($^{16}O^{2-}$) and new lattice oxygen ($^{18}O^2$) from the Cu ions is quickly exchanged and replenished in oxygen vacancy by gaseous $^{18}O_2$ all the time so that the dispersed CuO species is formed on the Cu_2O-CC surface. Therefore, the rapid formation of $C^{16}O_2$ and $C^{16}O^{18}O$ by the reaction of adsorbed CO and lattice oxygen ($^{16}O^{2-}$ and $^{18}O^{2-}$) over Cu_2O-CC mainly follows the Mars-van Krevelen (M-K) mechanism. However, some adsorbed oxygen cannot transform to lattice oxygen and still remains on the Cu_2O-CC surface, thus slow the increasing of $C^{18}O_2$, which tends to be formed by the reaction of adsorbed CO on the Cu^+ and partially adsorbed oxygen ($^{18}O^-/^{18}O_2^-/^{18}O_2^{2-}$) from Cu^{2+} *via* the dissociation of $^{18}O_2$, and following the L-H mechanism [35]. The same mechanism was also verified by the modest reaction energy barrier of adsorbed CO and adsorbed oxygen species from the DFT results.

Fig. 9 (B) showed the three reaction stages including first reduction (10 vol% CO/Ar), oxidation (21 vol% $^{18}O_2$/Ar) and the second reduction (10 vol% CO/Ar) over Cu_2O catalyst to investigate the CLC process. The pure Ar was purged with about 10 min to remove reactants existed in the reactor after reaching stable state of each reaction stage. For the first reduction stage, the only product was $C^{16}O_2$ which decreased to 0, attributed to continuous until complete consumption of surface lattice oxygen in Cu_2O-CLC due to no extra supplement of gaseous oxygen. Then the gaseous $^{18}O_2$ was added for oxidation reaction stage. It can also be seen from Fig. 9B that the concentration of $^{18}O_2$ was delayed reaching to 21 vol% due to the facile oxidation process of Cu^0 to Cu^+ and/or Cu^{2+}. On the other hand, the concentration of $^{18}O_2$ is quickly increased to 21 vol% with no delay and maintain stability in the CC reaction (Fig. 9 A) under the same switching operation, indicating that there is no evident effect of dead volume. The evident amount of $^{16}O_2$ produces firstly and decreases to zero nearly, illustrating that some lattice oxygen migrates from bulk to surface of the catalyst. Many reports have demonstrated that bulk oxygen can migrate to the surface and participate in the CO oxidation reaction [36]. Furthermore, at second reduction stage, $C^{16}O_2$ quickly produced again attributed to the bulk lattice oxygen ($^{16}O^{2-}$) of Cu_2O migrated to the surface after the substitution and activation of gaseous $^{18}O_2$, and participate in the reaction with dominant M-K mechanism, which is also demonstrated by other groups [35]. Compared the continuous stable generation of $C^{16}O_2$ (0.7 vol%) over Cu_2O-CC (Fig. 9 A), the $C^{16}O_2$ quickly increases and then decreases to zero on the Cu_2O-CLC in the reaction stage (Fig. 9 B), suggesting that the former can realize a steady migrating and reacting process from bulk lattice oxygen ($^{16}O^{2-}$) to surface lattice oxygen ($^{16}O^{2-}$) of catalyst itself under the coactivation of gaseous oxygen. The effective substitution of lattice $^{16}O^{2-}$ by $^{18}O^{2-}$ in the oxygen vacancy of Cu_2O-CLC catalyst and reaction with adsorbed CO on the interface are well verified by the rapid formation of $C^{16}O^{18}O$, which is in accordance with the M-K mechanism. The amount of detected $C^{18}O_2$ was small, thus the function of L-H mechanism is minimal.

The origins of different active oxygen species and corresponding mechanisms were qualitatively determined by using the isotopic exchange results (from Fig. 9A and B). In order to realize the quantitative analysis for CC and CLC reactions, the amount of different active oxygen species, the turnover frequency (TOF) and the contributions of M-K and L-H mechanisms to these reactions were calculated by the convolution integral of peak area in different products and Eq. (5) [35], as follows:

The two oxygen atoms derived from catalyst to form $^{16}O^{16}O$ and $C^{18}O^{18}O$,

$$mo = \frac{2 \times F_{to} \times A_{iO}}{100 \times m_{Cat} \times V_{gas}} \quad (3)$$

The one oxygen atom derived from catalyst to form $C^{16}O^{16}O$ and $C^{16}O^{18}O$,

$$mo = \frac{F_{to} \times A_{iO}}{100 \times m_{Cat} \times V_{gas}} \quad (4)$$

where m_O is the amount of different active oxygen species uptake of catalyst in mmol/g_{cat}; F_{to} is the total flow rate of gas in 0.03 L/min; A_{io} is the peak area of gaseous product in %·min based on the isotopic exchange results; m_{Cat} is the mass of catalyst in 0.03 g; V_{gas} is the gas molar volume with a given temperature (300 °C) under normal atmosphere, L/

mmol.

$$TOF(S^{-1}) = \frac{X_{Co2} \times F_{CO}}{mo \times m_{Cat}} \quad (5)$$

where X_{CO2} is the different types of CO_2 yield at a given temperature, F_{CO} is the flow rate of CO in mol/s, m_{Cat} is the mass of catalyst in g; m_O is the amount of different active oxygen species uptake of catalyst in mmol/g_{cat}.

The amount of three active oxygen species from the different active sites including bulk lattice oxygen ($^{16}O^{2-}$) from Cu^{+}, surface cycle lattice oxygen ($^{18}O^{2-}$) from $Cu^{+/2+}$ and adsorbed oxygen ($^{18}O^{-}/^{18}O_2^{-}/^{18}O_2^{2-}$) from Cu^{2+} were 8.46, 1.79 and 0.81 mmol/g_{cat}, respectively, and given in Fig. 9(C). The TOF of surface cycle $^{18}O^{2-}$ was higher among all three oxygen species, which revealed that the intrinsic activity of surface cycle $^{18}O^{2-}$ is rather prominent and reacts with adsorbed CO to form a lot of $C^{16}O^{18}O$ although its amount was only 1.79 mmol/g_{cat}. It is clearly observed that the TOF of surface cycle $^{18}O^{2-}$ in the Cu_2O-CC (13.5×10^{-3} s^{-1}) is larger than that of Cu_2O-CLC (4.7×10^{-3} s^{-1}), but reverse trend was observed for bulk $^{16}O^{2-}$ species. The reason is that the CO was mainly oxidized by surface lattice oxygen and new surface $^{18}O^{2-}$ continually exchanged and replenished by gaseous $^{18}O_2$ all the time, and then the CuO layer was gradually formed to enhance turnover rate and thus form much $C^{16}O^{18}O$ on the surface of Cu_2O in CC, verified by the SEM results (Fig. 5B). However, the collapse of cubic Cu_2O structure and agglomeration of CuO in CLC as shown in Fig. 5C were liable to expose more bulk $^{16}O^{2-}$ to participate in the reaction, resulting in the TOF of bulk $^{16}O^{2-}$ of Cu_2O-CLC higher than that of Cu_2O-CC. The continuous coactivation of excess gaseous $^{18}O_2$ tends to form more adsorbed oxygen species for Cu_2O-CC, whereas there is no gaseous $^{18}O_2$ to accelerate reaction for Cu_2O-CLC. Hence the former exhibits the higher TOF of adsorbed oxygen than the latter.

The contributions of M-K and L-H mechanisms to CO oxidation were calculated and displayed in Fig. 9(D). For the CC on Cu_2O, the degree of contribution of surface cycle lattice $^{18}O^{2-}$ (69.4%) for M-K pathway was dominated, followed by the L-H mechanism with the contributions of adsorbed oxygen (23.4%). But the role of bulk lattice $^{16}O^{2-}$ was

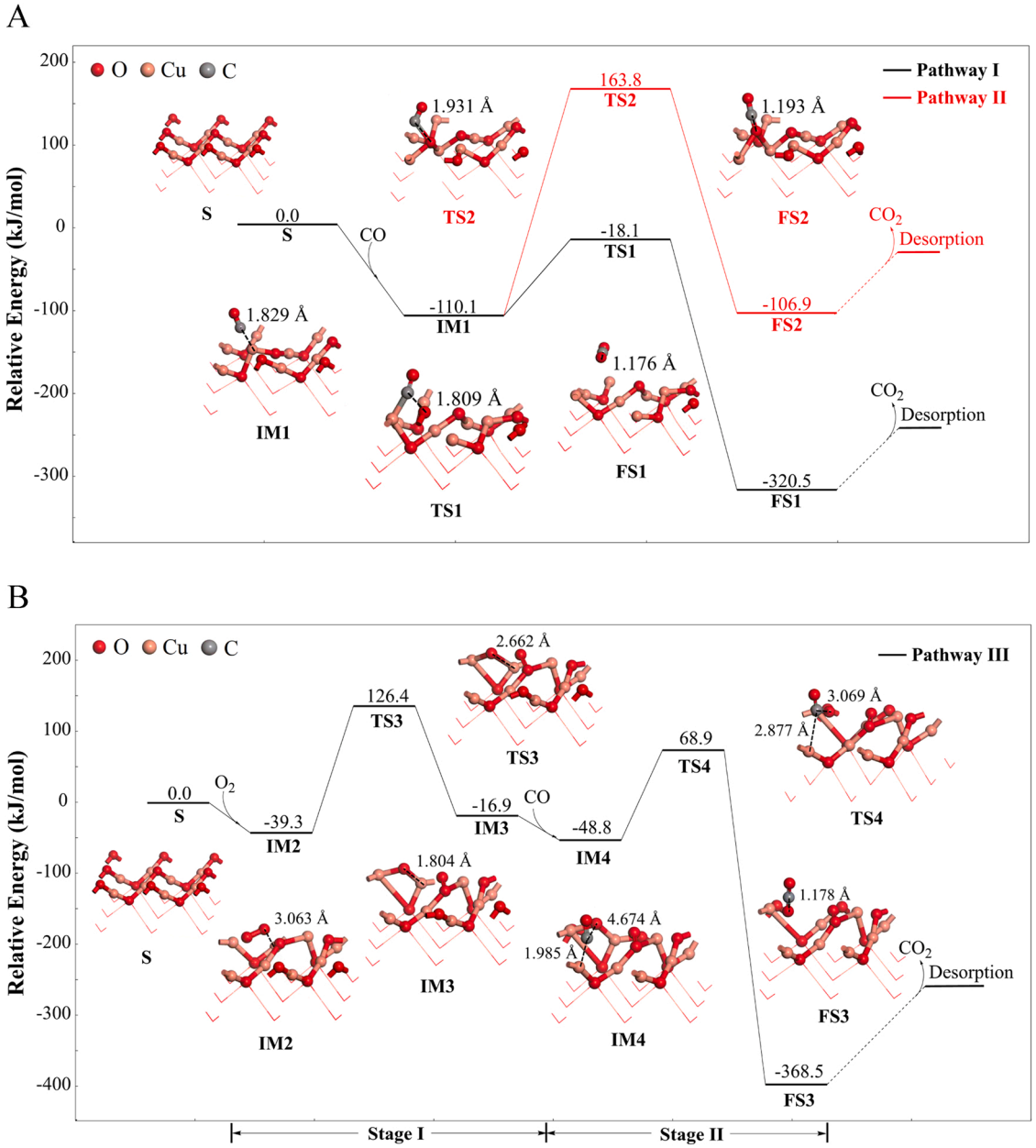

Fig. 10. Oxidation pathways of CO over Cu_2O (100) surface.

dominated for CLC reaction. Both surface cycle $^{18}O^{2-}$ (45.4%) and bulk $^{16}O^{2-}$ (44.3%) were almost contributed equally to M-K mechanism for CLC reaction, though the contribution degree of adsorbed oxygen (10.3%) was small to ignore the function of L-H mechanism.

3.4. DFT results

In order to explore and verify the detailed mechanisms of CO catalytic oxidation, the stable optimized structures and adsorption behavior of CO on the four potential sites of the Cu_2O (100) were firstly calculated, named as 1 A~D, respectively. As for the CO adsorption with C-end or O-end on the Cu_2O surface, corresponding stable structures were performed as shown in Fig. S5. In 1 A–C configurations, the distance between CO and surface oxygen atoms was more than 3.3 Å, and the surfaces have no obvious deformation with adsorption energy ranges from −7.1 to −12.8 kJ/mol, controlled by physical adsorption. In 1D configuration, C atom is adsorbed on Cu-site and the distance between C atom and surface Cu atom is only 1.829 Å. The CO molecule tends to adsorb on the surface with C-down orientation, which attributes to the components of the 5σ and 2π* orbitals of adsorbed C atom from CO [37]. The surface Cu atoms with obvious displacement releasing the adsorption energy of −110.12 kJ/mol, was controlled by chemical adsorption. Prior to adsorb on surface Cu atom to form copper carbonyl, it reacts with active O atom, and thus oxygen atoms coordinated with copper have higher reactivity.

The catalytic oxidation pathways of CO over Cu_2O(100) surface were performed to investigate the interaction between adsorbed CO and three different oxygen species as shown in Fig. 10. The pathway I in Fig. 10(a) is the reaction between adsorbed CO and surface lattice O, and pathway II is the reaction between adsorbed CO and lattice O in bulk phase. In pathway I, CO is chemically adsorbed on the surface Cu site forming IM1 with the energy of −110.1 kJ/mol, and then reacts with the surface lattice O atom of the first layer to form C—O bond in the transition state (TS1). CO_2 (FS1) is formed, wherein the energy barrier is only 92.0 kJ/mol. In this pathway, the adsorbed CO reacts with a surface lattice oxygen to generate a CO_2 molecule, which follows M-K mechanism [38]. Similarly, CO is firstly adsorbed on the surface Cu site (IM1) in pathway II, bonding with the bulk lattice O atom in the third layer (TS2), and then forming CO_2 (FS2). The energy barrier of the complete reaction process is 273.9 kJ/mol, which is much higher than pathway I, and also controlled by the M-K mechanism. In pathway III (Fig. 10b), the oxidation of CO is divided into two stages, one is the adsorption and dissociation of O_2, and the other is the CO oxidation. In stage I, O_2 is adsorbed on the surface to form IM2, and then dissociates and forms two adsorbed O atoms (IM3) going through TS3. Subsequently, CO is adsorbed on the surface Cu site (IM4) in stage II, gradually approaching one of the adsorbed O atom (TS4), and finally a C—O bond is generated, forming CO_2 (FS3). The whole reaction process needs to overcome the energy barrier of 117.7 kJ/mol, and the reaction heat is −368.5 kJ/mol, which follows the L-H mechanism. Based on the above results, the reaction energy barrier of three pathways is in the order of pathway II (273.9 kJ/mol) > pathway III (117.7 kJ/mol) > pathway I (92.0 kJ/mol), suggested that the adsorbed CO with surface lattice O in Pathway I is the most likely easy to occur on the cubic Cu_2O catalyst, whereas pathway II involved the adsorbed CO with bulk lattice O which was likely to be more difficult. The calculated values of the interaction between adsorbed CO and three different oxygen species were consistent with the isotopic exchange results.

3.5. Discussion

3.5.1. Intrinsic interface effect in structure-activity relationship

The evolution behaviors of catalyst structure was exhibited a significant effect on the catalytic activity and stability. Few unstable surface Cu_2O was oxidized to CuO species over Cu_2O in CC process, whereas the cubic structure with typical crystal planes (100) of the Cu_2O was not stable during CLC process as confirmed by XRD and SEM results. The excellent activity of Cu_2O for CC reaction was attributed to the stable cubic Cu_2O structure and its optimal metal-oxide interface (Cu^+/Cu^{2+}-[O]), which were contributed to the acceleration of the CO adsorption and/or the rate of active oxygen exchange. The suitable non-stoichiometric CuO_x species formed on the cubic Cu_2O-CC surface with a brisk interaction effect ($Cu^+ \leftrightarrow Cu^{2+}$) induces long-range charge transfer and thereby causes rapid oxygen delivery under the stable electric field. Then valence variation of copper is accompanied by a cycle change in the number of surface lattice oxygen ions and species transformations of copper oxides. The electronic interactions always occur at reactive interfaces (CuO-Cu_2O), and are simply driven by the principles of the system energy minimization and the continuity of the electric potential in a solid [39,40]. It occurs a cyclic and synergetic effect of non-stoichiometric CuO_x species ($Cu^+ \leftrightarrow Cu^{2+}$) on the concomitant CuO-Cu_2O interfaces, which is also detected on the used Cu_2O-CC catalyst, according to the XPS results. But for Cu_2O-CLC, there are no evident crystal planes of the Cu_2O structure due to collapse of the cubic Cu_2O structure. The agglomeration of CuO_x cannot provide a good cubic interface between the Cu ions and active oxygen species, resulting in the gradual decrease of reaction stability during the CLC reaction, which cannot be recovered even in oxygen-rich ambient. At the same time, too much CuO species was formed on the CuO-Cu_2O interfaces over the used Cu_2O-CLC catalyst. In this way, the total perimeter length of cubic interface on the Cu_2O-CC is bigger than that of Cu_2O-CLC, as confirmed by the size decreasing of single cube from Cu_2O-CC to Cu_2O-CLC by SEM morphology results. Such an interface structure change behavior is typical for evolution of two-dimensional islands involving bond-breaking at the edge sites and switching of active oxygen atom [41–43]. The TOF value of surface lattice oxygen on the Cu_2O-CC (13.5×10^{-3} s^{-1}) is much higher than that of Cu_2O-CLC (4.8×10^{-3} s^{-1}) (Fig. 9A), acted as crucial reaction step to improve the Cu_2O-CC activity. Therefore, the effective cubic metal-oxide interface over the Cu_2O-CC can be more energetically afford a platform to promote CO catalytic oxidation because of its excellent ability to transport surface lattice oxygen and copper ions.

3.5.2. The roles of different active oxygen species in the reaction pathways

The transformation and cycle of active oxygen species on cubic Cu_2O are the key factor in the CC and CLC reactions. According to the O_2-TPD and isotopic exchange results, the adsorbed oxygen, surface lattice oxygen and bulk lattice oxygen were confirmed as the active oxygen species in the cubic Cu_2O. The supplied gaseous oxygen fills the oxygen vacancies and contributes to exchange and replenishment of lattice oxygen in CO oxidation reaction. Based on the knowledge of the literatures, the exchange between gaseous O_2 and solid catalyst includes homoexchange and heteroexchange, which can be described as gas–gas exchange and gas–solid exchange, respectively [44,45]. The CC reaction process is proposed in three pathways as shown in Scheme 1 and can be depicted as follows. Firstly, O_2 is dissociated into O atoms, which were adsorbed in the oxygen vacancies of Cu_2O surface. A small part of adsorbed oxygen species (O_{ad}) can react directly with adsorbed CO species at an intermediate rate (TOF=10.0×10^{-3} s^{-1}), in accordance with L-H mechanism. In this process, the exchange of oxygen species is the homoexchange. Surface cycle lattice oxygen (O_{scl}, TOF=13.5×10^{-3} s^{-1}) rapidly participates in the reaction as main active oxygen species follow the M-K mechanism and are replenished by adsorbed oxygen species being incorporated into the lattice *via* surface vacancies. Then migration and transformation of oxygen species make a cycle of O_{scl} and play a dominant contribution degree (69.4%) during CO catalytic combustion process, since heteroexchange involves one or two oxygen atoms of the solid simultaneously [46,47]. Finally, a little of effective internal bulk lattice oxygen (O_{bl}, TOF=0.3×10^{-3} s^{-1}) can take part in the reaction with M-K mechanism slowly because the interface reaction mainly occurs on the smooth cubic Cu_2O surface. However, there are some differences in the CLC reaction process because of different

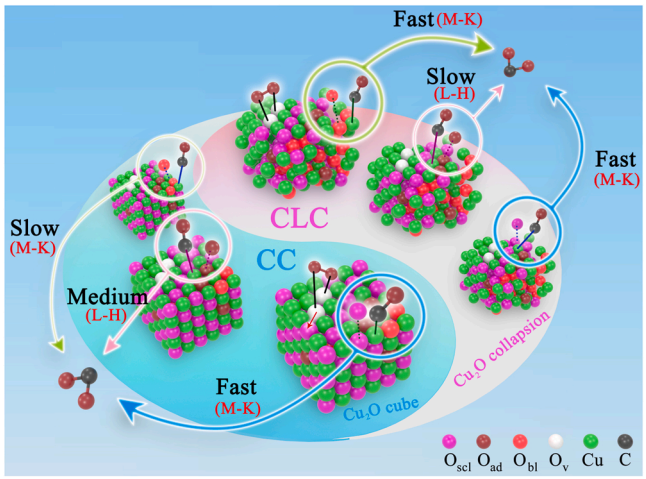

Scheme 1. Reaction pathways for CC and CLC processes over Cu_2O catalyst.

reaction conditions as shown in in Scheme 1. A small of residual adsorbed oxygen species after 21 vol% $^{18}O_2$ oxidations can react with adsorbed CO at a slow rate (TOF=2.4 × 10^{-3} s^{-1}). Compared to the surface cycle lattice oxygen, however, the bulk lattice oxygen makes a similar contribution degree for M-K mechanism with a total fast reaction rate. The fact is that CuO_x collapsion and agglomeration of Cu_2O expose in gas-solid phase interface and promoting the migration of bulk lattice oxygen during the CLC process, demonstrated by $^{18}O_2$ exchange experiments. This phenomenon reveals the nature of bulk lattice oxygen in the Cu_2O-CLC, which can be readily "pumped out" by structure collapse and much CuO_x formation *via* a back-spillover effect [48]. From a fundamental point of view, this behavior falls in the framework of the generalized Cabrera–Mott theory [49,50]. It also indicates that the heteroexchange is not only confined to the surface gas–solid reaction, but also occurs in the bulk gas–solid reaction during the different reaction conditions. Hence, besides surface lattice oxygen, bulk lattice oxygen can be effective during the CLC reaction process.

4. Conclusion

The cubic Cu_2O model catalyst was prepared to reveal the evolution behaviors and the contribution of different reaction mechanisms for CC and CLC. The catalytic activity and stability on Cu_2O for CC process were outperformed as compared to that of CLC process. The XRD, XPS, SEM and TPR/TPD analysis suggested that the high electronic interactions effect ($Cu^{+}\leftrightarrow Cu^{2+}$) on the reactive metal-oxide interface (100) to promote the CC reaction over Cu_2O, though few unstable surface Cu_2O was oxidized to CuO species. On the other hand, Cu_2O structure was collapsed with agglomerated CuO_x species during CLC process. The reaction pathways and three different active oxygen species including surface cycle lattice oxygen, bulk lattice oxygen, and adsorbed oxygen were clearly verified *via in situ* IR, isotopic ($^{18}O_2$) transient exchange and DFT calculation. The intrinsic activity of surface cycle lattice oxygen was higher with TOF of 13.5 × 10^{-3} s^{-1} and reacts with adsorbed CO to form a lot $C^{16}O^{18}O$ over Cu_2O-CC, abided by M-K mechanism. The bulk lattice oxygen ($^{16}O^{2-}$) from bulk Cu_2O can evidently migrate to the surface after the substitution and activation of gaseous $^{18}O_2$ to form $C^{16}O^{16}O$ on the Cu_2O-CLC, also followed M-K mechanism. The slow incremental in the formation of $C^{18}O_2$ was observed from the reaction of adsorbed CO and partially adsorbed oxygen ($^{18}O^{-}$/$^{18}O_2^{-}$/$^{18}O_2^{2-}$) that slightly in accordance with L-H mechanism. The obtained contributions of M-K and L-H mechanistic pathways for CC and CLC processes were 76.6% and 23.4% on Cu_2O-CC, as well 89.7% and 10.3% on Cu_2O-CLC, respectively.

CRediT authorship contribution statement

Running Kang: Design, Data curation, Formal analysis, Investigation, Writing – original draft. **Junqin Huang**: Data curation, Formal analysis. **Zihao Teng**: Methodology. **Xiaolin Wei**: Supervision, Resources, Project administration. **Feng Bin**: Supervision, Results discussion, Funding acquisition, Writing – eview & editing. **Baojuan Dou**: Methodology, Investigation, Writing – review & editing. **Saravanan Kasipandi:** Writing – review & editing and investigation of reaction mechanism study.

Declaration of Competing Interest

The authors declare that they have no known competing financial interests or personal relationships that could have appeared to influence the work reported in this paper.

Acknowledgments

We gratefully acknowledge the financial support from the National Natural Science Foundation of China (No. 52176141), China Scholarship Council (No. 202004910623), and DFT simulation in 2021 from CSC-IT Center for Science, Finland, for computational resources.

Appendix A. Supplementary material

Supplementary data associated with this article can be found in the online version at doi:10.1016/j.apcatb.2022.121296.

References

[1] R.N. Kang, X.L. Wei, P.D. Ma, F. Bin, J.Y. He, Q.L. Hao, B.J. Dou, Self-sustained combustion of CO with transient changes and reaction mechanism over $CuCe_{0.75}Zr_{0.25}O_\delta$ powder for honeycomb ceramic catalyst, Fuel 263 (2020), 116637.
[2] J. Adánez, A. Abad, Chemical-looping combustion: status and research needs, Proc. Combust. Inst. 37 (2019) 4303–4317.
[3] J. Adánez-Rubio, P. Gayán, A. Abad, F. García-Labiano, L.F. de Diego, J. Adánez, Kinetic analysis of a Cu-based oxygen carrier: relevance of temperature and oxygen partial pressure on reduction and oxidation reactions rates in chemical looping with oxygen uncoupling (CLOU), Chem. Eng. J. 256 (2014) 69–84.
[4] F. Bin, X.L. Wei, B. Li, K.S. Hui, Self-sustained combustion of carbon monoxide promoted by the Cu-Ce/ZSM-5 catalyst in $CO/O_2/N_2$ atmosphere, Appl. Catal. B Environ. 162 (2015) 282–288.
[5] B. Li, Y. Duan, D. Luebke, B. Morreale, Advances in CO_2 capture technology: a patent review, Appl. Energy 102 (2013) 1439–1447.
[6] F. Bin, R.N. Kang, X.L. Wei, Q.L. Hao, B.J. Dou, Self-sustained combustion of carbon monoxide over $CuCe_{0.75}Zr_{0.25}O_\delta$ catalyst: stability operation and reaction mechanism, Proc. Combust. Inst. 37 (4) (2019) 5507–5515.
[7] F. Liu, J. Liu, Y.J. Yang, Z. Wang, C.G. Zheng, Reaction mechanism of spinel $CuFe_2O_4$ with CO during chemical-looping combustion: an experimental and theoretical study, Proc. Combust. Inst. 37 (2019) 4399–4408.
[8] X. Tian, M.Z. Su, H.B. Zhao, Kinetics of redox reactions of $CuO@TiO_2$–Al_2O_3 for chemical looping combustion and chemical looping with oxygen uncoupling, Combust. Flame 213 (2020) 255–267.
[9] T.J. Huang, D.H. Tsai, CO oxidation behavior of copper and copper oxides, Catal. Lett. 87 (2003) 173–178.
[10] R.N. Kang, X.L. Wei, F. Bin, Z.B. Wang, Q.L. Hao, B.J. Dou, Reaction mechanism and kinetics of CO oxidation over a $CuO/Ce_{0.75}Zr_{0.25}O_{2-\delta}$ catalyst, Appl. Catal. A Gen. 565 (2018) 46–58.
[11] R.N. Kang, P.D. Ma, J.Y. He, H.X. Li, F. Bin, X.L. Wei, B.J. Dou, K.N. Hui, K.S. Hui, Transient behavior and reaction mechanism of CO catalytic ignition over a CuO–CeO_2 mixed oxide, Proc. Combust. Inst. 38 (2021) 6493–6501.
[12] P.D. Ma, Z.H. Teng, Q.L. Hao, R.N. Kang, B. L, F. Bin, B.J. Dou, Effects of precursor concentration on morphologies of Cu_2O micro/nanocrystals and properties of CO self-sustained catalytic combustion, Fuel 289 (2021), 119776.
[13] Q. Hua, T. Cao, H.Z. Bao, Z.Q. Jiang, W.X. Huang, Crystal-plane-controlled surface chemistry and catalytic performance of surfactant-free Cu_2O nanocrystals, ChemSusChem 6 (2013) 1966–1972.
[14] E.A. Goldstein, R.E. Mitchell, Chemical kinetics of copper oxide reduction with carbon monoxide, Proc. Combust. Inst. 33 (2011) 2803–2810.
[15] C.K. Clayton, H.Y. Sohn, K.J. Whitty, Oxidation kinetics of Cu_2O in oxygen carriers for chemical looping with oxygen uncoupling, Ind. Eng. Chem. Res. 53 (2014) 2976–2986.
[16] M.Z. Su, J. Cao, X. Tian, Y.L. Zhang, H.B. Zhao, Mechanism and kinetics of Cu_2O oxidation in chemical looping with oxygen uncoupling, Proc. Combust. Inst. 37 (2019) 4371–4378.

[17] Z.H. Zhang, H. Wu, Z.Y. Yu, R. Song, K. Qian, X.Y. Chen, J. Tian, W.H. Zhang, W. X. Huang, Site-resolved Cu_2O catalysis in the oxidation of CO, Angew. Chem. Int. Ed. 58 (13) (2019) 4276–4280.
[18] L.N. Wu, Z.Y. Tian, A.E. Kasmi, M.F. Arshad, W. Qin, Mechanistic study of the CO oxidation reaction on the CuO (111) surface during chemical looping combustion, Proc. Combust. Inst. 38 (2021) 5289–5297.
[19] A. Chen, X.J. Yu, Y.Y. Zhou, S. Miao, Y. Li, S. Kuld, J. Sehested, J.Y. Liu, T. Aoki, S. Hong, M.F. Camellone, S. Fabris, J. Ning, C.C. Jin, C.W. Yang, A. Nefedov, C. WÖll, Y.M. Wang, W.J. Shen, Structure of the catalytically active copper–ceria interfacial perimeter, Nat. Catal. 2 (2019) 334–341.
[20] B. Delley, An all-electron numerical method for solving the local density functional for polyatomic molecules, J. Chem. Phys. 92 (1990) 508–517.
[21] J.P. Perdew, K. Burke, M. Ernzerhof, Generalized gradient approximation made simple, Phys. Rev. Lett. 77 (1996) 3865–3868.
[22] J.P. Perdew, K. Burke, Y. Wang, Generalized gradient approximation for the exchange-correlation hole of a many-electron system, Phys. Rev. B 54 (1996) 16533–16539.
[23] A.A. Hssi, L. Atourki, N. Labchir, et al., Structural and optical properties of electrodeposited Cu_2O thin films, Mater. Today Proc. 22 (2020) 89–92.
[24] T.H. Fischer, J. Almlof, General methods for geometry and wave function optimization, J. Phys. Chem. 96 (1992) 9768–9774.
[25] H.Z. Bao, W.H. Zhang, Q. Hua, Z.Q. Jiang, J.L. Yang, W.X. Huang, Crystal-plane-controlled surface restructuring and catalytic performance of oxide nanocrystals, Angew. Chem. Int. Ed. 50 (51) (2011) 12294–12298.
[26] D.F. Zhang, H. Zhang, L. Guo, K. Zheng, X.D. Han, Z. Zhang, Delicate control of crystallographic facet-oriented Cu_2O nanocrystals and the correlated adsorption ability, J. Mater. Chem. 19 (2009) 5220–5225.
[27] K. Wang, Q.B. Yu, Q. Qin, Reduction kinetics of Cu-based oxygen carriers for chemical looping air separation, Energy Fuels 27 (2013) 5466–5474.
[28] Y.N. Gao, L. Zhang, A.J.F. van Hoof, E.J.M. Hensen, On the surface-dependent oxidation of Cu_2O during CO oxidation: Cu^{2+} is more active than Cu^{+}, Appl. Catal. A Gen. 602 (2020), 1177122.
[29] Y.N. Zheng, K.Z. Li, H. Wang, H. Wang, D. Tian, Y.G. Wei, X. Zhu, C.H. Zeng, Y. M. Luo, Structure dependence and reaction mechanism of CO oxidation: a model study on macroporous CeO_2 and CeO_2–ZrO_2 catalysts, J. Catal. 344 (2016) 365–377.
[30] Y. Yang, S. Zhang, S. Wang, K. Zhang, H. Wang, J. Huang, S. Deng, B. Wang, Y. Wang, G. Yu, Ball milling synthesized MnO_x as highly active catalyst for gaseous POPs removal: significance of mechanochemically induced oxygen vacancies, Environ. Sci. Technol. 49 (2015) 4473–4480.
[31] J. Jia, P. Zhang, L. Chen, Catalytic decomposition of gaseous ozone over manganese dioxides with different crystal structures, Appl. Catal. B Environ. 189 (2016) 210–218.
[32] T. Andana, M. Piumetti, S. Bensaid, N. Russo, D. Fino, Heterogeneous mechanism of NOx-assisted soot oxidation in the passive regeneration of a bench-scale diesel particulate filter catalyzed with nanostructured equimolar ceria-praseodymia, Appl. Catal. A Gen. 583 (2019), 117136.
[33] T. Andana, M. Piumetti, S. Bensaid, L. Veyre, C. Thieuleux, N. Russo, D. Fino, E. A. Quadrelli, R. Pirone, Nanostructured equimolar ceria-praseodymia for NOx-assisted soot oxidation: insight into Pr dominance over Pt nanoparticles and metal–support interaction, Appl. Catal. B Environ. 226 (2018) 147–161.
[34] C. Serre, F. Garin, G. Belot, G. Maire, Reactivity of Pt/Al_2O_3 and $Pt\text{-}CeO_2Al_2O_3$ catalysts for the oxidation of carbon monoxide by oxygen: I. Catalyst characterization by TPR using CO as reducing agent, J. Catal. 141 (1993) 1–8.
[35] Y. Qin, H. Wang, C. Dong, Z.P. Qu, Evolution and enhancement of the oxygen cycle in the catalytic performance of total toluene oxidation over manganese-based catalysts, J. Catal. 380 (2019) 21–31.
[36] S. Liu, X. Wu, W. Liu, W. Chen, R. Ran, M. Li, D. Weng, Soot oxidation over CeO_2 and Ag/CeO_2: factors determining the catalyst activity and stability during reaction, J. Catal. 337 (2016) 188–198.
[37] F. Liu, J. Liu, Y. Yang, X. Wang, A mechanistic study of CO oxidation over spinel $MnFe_2O_4$ surface during chemical-looping combustion, Fuel 230 (2018) 410–417.
[38] T.G. Mi, Y.W. Wu, M.X. Xu, X.Y. Zhou, B. Hu, L. Zhao, Q. Lu, Theoretical insights into the roles of active oxygen species in heterogeneous oxidation of CO over Mn/TiO_2 catalyst, Appl. Catal. A Gen. 616 (2021), 118104.
[39] R.T. Tung, Recent advances in Schottky barrier concepts, Mater. Sci. Eng. R 35 (2001) 1–138.
[40] J.J. Wang, T.J. Fu, F.H. Meng, D. Zhao, S.S.C. Chuang, Z. Li, Highly active catalysis of methanol oxidative carbonylation over nano Cu_2O supported on micropore-rich mesoporous carbon, Appl. Catal. B Environ. 303 (2022), 120890.
[41] Z.J. Wang, J. Dong, Y. Cui, G. Eres, O. Timpe, Q. Fu, F. Ding, R. Schloegl, M. G. Willinger, Stacking sequence and interlayer coupling in few-layer graphene revealed by in situ imaging, Nat. Commun. 7 (2016) 13256.
[42] K. Zhang, L.F. Li, S. Shaikhutdinov, H.J. Freund, Carbon monoxide oxidation on metal-supported monolayer oxide films: establishing which interface is active, Angew. Chem. Int. Ed. 57 (2018) 1261–1265.
[43] S. Lee, C. Lin, S. Kim, X.Y. Mao, T. Kim, S.J. Kim, R.J. Gorte, W.C. Jung, Manganese oxide overlayers promote CO oxidation on Pt, ACS Catal. 11 (2021) 13935–13946.
[44] Y. Huang, C. Pellegrinelli, E. Wachsman, Oxygen dissociation kinetics of concurrent heterogeneous reactions on metal oxides, ACS Catal. 7 (2017) 5766–5772.
[45] C. Kan, E. Wachsman, Isotopic-switching analysis of oxygen reduction in solid oxide fuel cell cathode materials, Solid State Ion. 181 (2010) 338–347.
[46] U. Menon, V.V. Galvita, G.B. Marin, Reaction network for the total oxidation of toluene over $CuO\text{-}CeO_2/Al_2O_3$, J. Catal. 283 (2011) 1–9.
[47] A. Bueno-López, K. Krishna, M. Makkee, Oxygen exchange mechanism between isotopic CO_2 and Pt/CeO_2, Appl. Catal. A Gen. 342 (2008) 144–149.
[48] B.F. Jin, B.H. Zhao, S. Liu, Z.G. Li, K.X. Li, R. Ran, Z.C. Si, D. Weng, X.D. Wu, $SmMn_2O_5$ catalysts modified with silver for soot oxidation: dispersion of silver and distortion of mullite, Appl. Catal. B Environ. 273 (2020), 119058.
[49] N. Cabrera, N.F. Mott, Theory of the oxidation of metals, Rep. Prog. Phys. 12 (1949) 163.
[50] Q. Fu, T. Wagner, Interaction of nanostructured metal overlayers with oxide surface, Surf. Sci. Rep. 62 (2007) 431–498.